Horizon Detection from Electro-optical Sensors under Maritime Environment

Dong Liang, Ya Liang

***Abstract*—In recent years, target detection in maritime surveillance has become a popular subject. Horizon under maritime environment is one of the most important semantic boundaries for segmenting the image into sea and sky. With the help of horizon, seeking scope can be restricted to a definite small area which significantly reduces the computational complexity. Meanwhile horizon is used to automatically adjust the attitude of air vehicles as well. Although a plenty of algorithms for horizon detection have been created, they are prone to low visibility and occlusions. In this paper, a novel robust algorithm based on probability distribution and physical characteristics is proposed. At first the probabilities are distributed to each vertically divided region by weighted textures and the sea-sky region is located from definite probabilistic intervals. Based on Canny edge detector, Hough transform extracts a series of candidate horizons. Finally, a novel voting method is applied. The line with the maximum value will be regarded as the true horizon. The proposed algorithm can not only precisely detect the horizon from fine images but also from blurred image, even with splashed camera. The performance of the proposed algorithm is verified by experiments on 65 videos containing more than 20000 frames under different sceneries. The results illustrate that our algorithm can detect the horizon line with minor errors in comparison with other 5 state-of-the-art algorithms.**

***Index Terms*—Horizon detection, physical characteristics, maritime environment, contextual information, electro-optical sensor, sea-sky region extraction.**

I. Introduction

HORIZON detection under maritime circumstance has various applications. Nowadays large amount of researches have been carried out for detecting horizon [1]. As the marine vehicles in long range always appear near the horizon, the area for target search can be limited to the sea-sky region [2]-[7], [30]. It can not only significantly reduce the computational cost for searching targets, but also decrease the disturbance brought by illumination changes from sea wave or cloud clutters. Due to the limited payload, MAV (Micro Air Vehicle) prefers video camera which is lighter, smaller and requires less power. Besides, image with rich information contains more details. The pitch and bank attitude of MAV could be evaluated from the orientation and position of horizon in video images. The horizon is also used to make image registration for subsequent target tracking [2], [6]. There exist several mainstream algorithms for horizon detection and evaluation such as: color-based statistical model [2], [5], [7], [10], [13], [14], [16], [30], [33], edge phase encoding [3], pixels classification [9], [17], [19]-[22], [31], [33], linear feature [2], [4]-[6], [14], [15], [18], [24], [32], color intensity and gradient [4]-[6], [11], [24], [33], textural feature [8], [20], [21], region-growing [12] and other physical characteristics near the horizon [5], [15], [18]-[22], [24]. In general, the hybrid algorithm performs a higher accuracy rate but it also brings computational burden.

By adjusting bank angle and pitch angle, two-dimensional line parameter is established to indicate the hypothesized horizon line. Then the color as one of the most prominent features is used to construct the covariance matrix of sea region and sky region respectively. A criterion is proposed which contains determinants and their corresponding sum-of-eigenvalues of covariance matrices. The maximum optimization criterion indicates the real horizon [6], [16]. Fefilatyev *et al.* [2] use Hough transformation to find several largest peaks and their corresponding lines are selected as candidate horizon. For each candidate horizon, the pixels above the line are classified as sky and the pixels below the line are labeled as sea. Similar to the method in [16], RGB color-based matrices are constructed and the Bhattacharyya distance [27] is applied in evaluating the difference between the distribution of sky and sea. The line with the maximum difference is regarded as the final horizon. Suppose that the sky and sea have homogeneous color region and horizon is apparent, the sea-sky region is extracted by calculating the Bhattacharyya distance between the color vector of sea region and sky region. Then Canny edge detector is applied to multi-scale image independently. At last, Hough transform and least squares are used to estimate the horizon [30]. However, the method is affected evidently for that the distribution in the sea region and sky region are not always distinguished. Especially in blurred image, the color distribution tends to be uniformed and the horizon becomes unclear. Lipschutz *et al.* [7] introduced probability distribution functions (PDF) to describe the gray distribution of sea region and sky region. The true horizon line corresponds to the maximum Bhattacharyya distance between two histograms. Gershikov *et al* [5] compared five hybrid methods for horizon detection in marine images. It is concluded that the H-DE [16] method has the least height deviation while the method H-HC based on linear feature has the smallest angle deviation. Whereas the longest line is not always to be the real horizon under some circumstances, the H-HC may not detect the horizon line effectively. Meanwhile H-HC method is easily

Manuscript received July 24, 2018; revised October 25, 2018; accepted December 26, 2018. The Associate Editor coordinating the review process was Dr. Kurt Barbe. (Corresponding author: Dong Liang.)

D. Liang is with the Department of Computer Sciences, the National Technical University at Kharkiv, 61002, Ukraine (email: liangton@foxmail.com; leongdong@outlook.com).

Y. Liang is with Weihai Ocean Vocational College at Weihai, 264300, China (email: 328365932@qq.com).

Color versions of one or more of the figures in this paper are available online at http://ieeexplore.ieee.org.

influenced by illumination distribution. In cloudy weather or with irregular sea wave, the accuracy of H-HC method decreases. Liu *et al*. [12] found the points where color changed in the leftmost and rightmost boundary respectively. According to the location of points, the virtual horizon is established. A rectangle region above virtual horizon is extracted as the region-growing seed. The region-growing algorithm will fill the entire sky region by calculating the color distance. Thus the final horizon is obtained from the least error classification method. Dumble *et al*. [11] investigated the characteristics such as color distribution, gradient information as well as spatial constraints. But these principles are not suitable for the maritime environment. Contrary to the ground region, the blue component in sea region is generally stronger than the red or green component. And the conclusion that negative gradient appears along the direction from sky to ground is not always correct. Some methods adopt classification to segment sky region from sea region. In [31], every pixel is classified into corresponding category using a pyramid scene-parsing neural network. The horizon is obtained by interactively applying least-squares regression along with median filtering. As a low-level feature, color is used to construct a support vector machine in [17]. In [33], combining gradient features, a line segment detection algorithm is proposed to build a candidate pool. With the similar assumptions as [30], the color vector consisting of mean, standard deviation as well as skewness, is used to determine the distance between two regions. Since the color is composed of several categories, training data is also calculated for fine detection. Finally the horizon is computed by RANSAC. Luo *et al*. [19]-[22] designed a model-based approach composed of color classification and physical-motivated signature validation, which is only effective in identical scenery with clear and light-blue sky at daytime. Besides classification methods always accompany with offline training that brings extra cost. Prasad *et al*. [32] builds weighted edge map based on multi-scale filter. And Radon transform extracts a series of candidate solutions. Parameter pair of every solution constructs the voting histograms. The bin with the maximum histogram count indicates the true horizon. An evident weakness of this method is that the precision is determined by the parameter pairs of solutions which are difficult to be controlled. More effectively, Prasad *et al*. [4] proposed a method for horizon detection called multi-scale cross modal linear feature. Based on multi-scale media filtering, the line is extracted by Hough transform as well as the intensity variation over different scales. Affirm score composed of geometric score and goodness score is computed. The highest value of affirm score indicates the true horizon line. The method can extract the horizon line accurately even from low-resolution image or under the environment that horizon is partially occluded by other objects. Also the method is prone to wave and its computational complexity is large.

This paper designs a hybrid method which consists of sea-sky region extraction and horizon estimation based on information of color, texture and context. At first the image is divided vertically into several equal sub-regions. Each sub-region is assigned with a probability which represents the possibility of being sea region. The belief map is constructed based on weighted textures while the sea-sky region is acquired by a specific interval of probability distribution. Then Canny edge detector and Hough transform are used to extract candidate lines. Finally, a novel voting method on the basis of the physical features around horizon is applied. The line with the maximal value will be regarded as the final horizon. According to the experimental results, the proposed method has a better performance than other existed methods especially under complex circumstances. Also, the proposed method has higher detection accuracy and processing rate.

II. Horizon Detection Algorithm

The sunlight passes through the air by absorption and scattering which are caused by air molecules [23], [28]. However the distribution of air particles is not uniform and the thickness of the medium is different. Bouger *et al*. [29] pointed that for the same medium, the thicker the medium is, the larger ratio of incident light to emergent light will be. The different intensity of emergent light constitutes sky texture. For sea region, the main surface light comes from reflection. The texture of sea region depends on the movement of wave and the altitude of sun. The distance from the horizon to observer is long enough that particles in the atmosphere scatter all colors almost equally. Moreover the sky region that is close to horizon contains more floating particles of vapor, which strengthen the scattering effect. The color distribution of sky region near the horizon tends to be uniform. Thus the complexity of texture on sky region near the horizon reduces to a low level. In [8], it had been proved by experimental results that sea region has more complex textural feature comparing to sky region under most environments. But for camera installed on MAV, the height of drone is high enough to cause sea region, which is next to horizon, as smooth as sky region. In this situation, textural feature is not adequate to discriminate sky region from sea sky. Thus color feature is introduced as weighted value of texture. According to Rayleighs law, the wave with long wavelength is scattered more weakly than the wave in short wavelength. Thus daylight sky often appears blue. But for twilight sky, the propagating distance increases to maximum for low position of the sun. Large proportion short lightwave is scattered out of beam causing orange red sky. Based on these characteristics, the horizon detection algorithm can be divided into two steps: the first step is sea-sky region extraction; the second step is horizon estimation. A flowchart of the proposed method shown in Fig. 1 is divided to 6 stages.

A. Sea-sky Region Extraction

As the spatial relationship is regarded as the function of distance between two pixels, the textural feature of region can be expressed by gray-level co-occurrence matrix [8]. At first, the original image is transformed from RGB color space to gray space. A one-pixel-wide vertical trace is randomly selected from the columns of original image. Then average values R_{avg} in red channel and B_{avg} in blue channel are

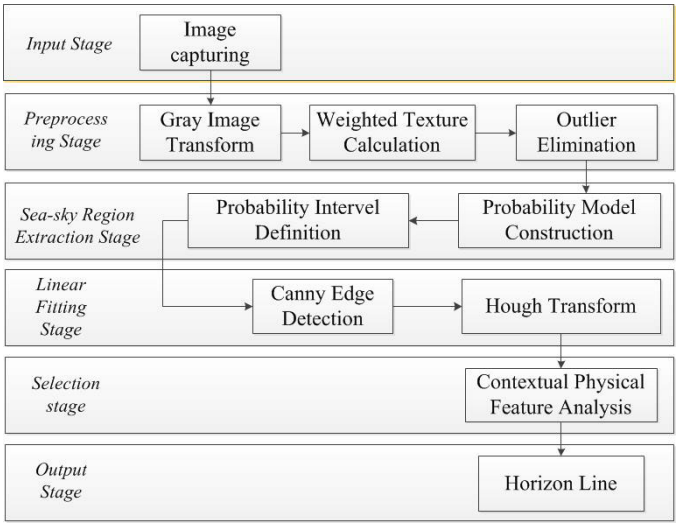

Fig. 1. Flowchart of proposed method.

calculated along the vertical trace respectively. The gray image is computed by following equation:

$$f(x,y) = \begin{cases} R(x,y) & \text{if} R_{avg} > B_{avg}, \\ B(x,y) & \text{else if} R_{avg} \leq B_{avg}. \end{cases} \quad (1)$$

where $f(x,y)$ is gray level at position (x,y) and $R(x,y)$, $B(x,y)$ represent respectively the values of red channel and blue channel in original image. The result of gray transformation is illustrated in Fig. 2.

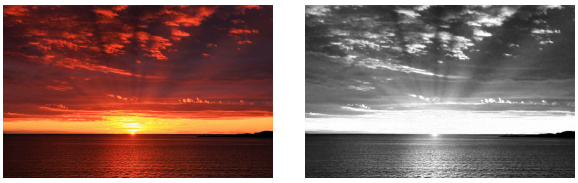

(a) Original image. (b) Gray image.

Fig. 2. The result of gray transformation

Before calculating textures of sea region and sky region, the gray image is divided equally into N ($N = 30$) sub-regions along vertical direction, which is shown at Fig. 3.

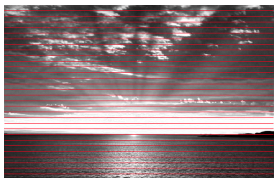

Fig. 3. The division of image along the vertical direction.

For each sub-region, a gray-level co-occurrence matrix is constructed, which is consisted of the joint numbers by combination of every two gray levels i and j along direction α, with distance d. The matrix is defined as:

$$p(i,j,d,\alpha) = \sharp\{[(x,y),(x+m,y+n)] \\ |f(x,y) = i, f(x+m,y+n) = j\} \quad (2)$$

where $m = d\cos\alpha$, $n = d\sin\alpha$, (x,y) and $(x+m,y+n)$ are positions of pixel pairs in image; $\sharp$ represents the amount of elements in the set; $\alpha(\alpha = 0°, 45°, 90°, 135°)$ denotes the angle between horizontal direction and the line connected by two pixels. To reduce the computational complexity, values are scaled from 8 bit to 4 bit. The scaled model is:

$$f(x,y) = f(x,y)/16 \quad (3)$$

A normalized matrix is defined as:

$$P(i,j,d,\alpha) = P(i,j,d,\alpha)/R \quad (4)$$

where R is the total number of pixel pairs. When the sea sky image is clear, there are significant differences between sea region and sky region in textural feature. However for blurred sea sky image, textural features of the two regions are confused while color feature performs better to differentiate sky from sea. A weighted correlation, which is inversely proportional to the second power of the average gray value, is proposed to quantify the complexity of regions for both clear and blurred image. The weighted texture calculation is presented:

$$WeCorr = \frac{1}{gray^2}(\sum_{i=1}^{L_1}\sum_{j=1}^{L_2} ijP(i,j) - \mu_x\mu_y)/\sigma_x\sigma_y \quad (5)$$

where $gray$ is the average gray value around the whole sub-region; $\mu_x = \sum_{i=1}^{L_1}\sum_{j=1}^{L_2} iP(i,j)$, $\mu_y = \sum_{i=1}^{L_1}\sum_{j=1}^{L_2} jP(i,j)$, $\sigma_x^2 = \sum_{i=1}^{L_1}\sum_{j=1}^{L_2}(i-\mu_x)^2P(i,j)$, $\sigma_y^2 = \sum_{i=1}^{L_1}\sum_{j=1}^{L_2}(j-\mu_y)^2P(i,j)$. L_1 is the number of co-occurrence matrix rows and L_2 corresponds to columns. Weighted textural value is calculated within each sub-region and is normalized by the maximum textural value. The histogram is illustrated in Fig. 4.

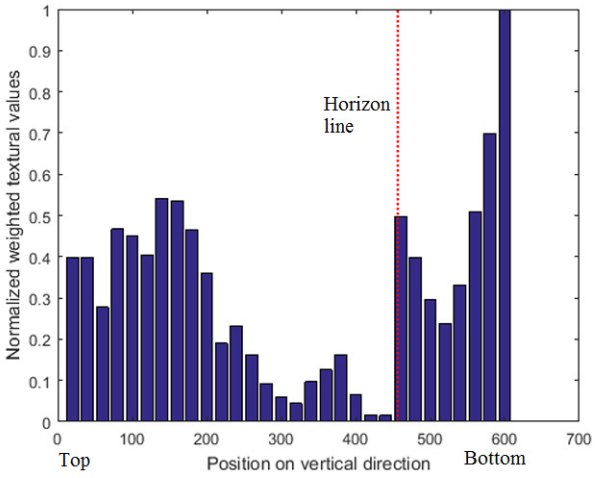

Fig. 4. Normalized weighted textural values (original). X axis describes the position of each sub-region on vertical direction and Y axis shows normalized weighted textural values.

Clouds with inhomogeneous thickness disturb the gray distribution over the sky region, which causes more complex textural feature. From Fig. 4, several sub-regions belonging to sky region have larger weighted textural values. Principles should be designed to modify these outliers. According to characteristics of sea-sky region around the horizon, the weighted textural values in sky region are smaller than the values in sea region as a result of scattering effect. It is supposed that 1) sea and sky have different weighted textural features; 2) the sub-region with the smallest weight textural value belongs to sky. By comparing to the average value and maximum value of weighted textural feature, a simple clustering algorithm is designed for region classification. The average weighted textural value is computed by:

$$WeCorr_{avg} = \frac{1}{N}\sum_{i=1}^{N} WeCorr(i) \tag{6}$$

The criteria for clustering is described as:

$$Pro(i) = \begin{cases} 0.0001 & if\ \frac{WeCorr_{avg}}{WeCorr(i)} > 2\ and \\ & \frac{WeCorr(i)}{WeCorr_{min}} < 10; \\ 0.9999 & elseif\ \frac{WeCorr(i)}{WeCorr_{avg}} > 1; \\ \frac{WeCorr(i)}{WeCorr_{avg}} & otherwise. \end{cases} \tag{7}$$

The sub-regions, appearing more like sea region, are classified into sea and assigned with 0.9999 as probability. On the contrary, the sub-regions having closer distance with sky region will be defined as sky in a low probability (0.0001). For other sub-regions, their probability of being sea will be determined by ratio of $WeCorr(i)$ and $WeCorr_{avg}$ For horizon line (red line of dashes) in Fig. 4, the sky region next to it has a lower weighted textural value which can be used to modify other upper sub-regions. From top to bottom, every sub-region will be assigned with a serial number in turns as 1, 2, 3,..., N. The probability value in the i^{th} sub-region would be modified by the $(i+1)^{\text{th}}$ sub-region, if i^{th} sub-region's probability is larger than the $(i+1)^{\text{th}}$ sub-region's probability; otherwise it executes do-nothing-operation. When no assignment operation appears over the whole traverse, the iteration is finished. The details of modifying process are presented as following pseudo codes.

This method can eliminate extreme outliers both in sky region and sea region. The histogram with verified probability is shown as Fig. 5. The boundary between sky and sea becomes evident. The sub-region which is more similar to sea has a larger probability while the sub-region which looks more like sky possesses a lower probability. The probability distribution appears S-shape and could be fitted by mathematical model. The consecutive mathematical model assigns probability to each row of image. And the sea-sky region is extracted by setting probability interval. A logistic model of sea is applied to making curve fitting. The logistic model is represented as:

$$f(x) = \frac{1}{1+e^{-(x-a)/c}} \tag{8}$$

where a is the offset of logistic function on x-axis. c represents the extent of inclination for curve: the value is higher; the curve is steeper. x is the location of seed region in original image. $f(x)$ is belief value corresponding to each x, $f(x)\epsilon(0,1)$. Suppose $y = ln(\frac{1}{f(x)} - 1)$. The logistic function is transformed to linear function as:

$$y = -\frac{x}{c} + \frac{a}{c} \tag{9}$$

Centre position x in each sub-region and probability y of corresponding sub-region are selected to construct a series of fitting points $\{[x(1), y(1)], [x(2), y(2)], \ldots, [x(N), y(N)]\}$. The method of least square, as an approach in linear regression, can be used in data fitting. Suppose $b(i) = ln\frac{1}{y(i)} - 1$. Then coefficients of linear function are calculated as:

$$-\frac{1}{c} = \frac{n\sum_{i=1}^{N} x(i)b(i) - \sum_{i=1}^{N} x(i)\sum_{i=1}^{N} b(i)}{n\sum_{i=1}^{N} x(i)^2 - (\sum_{i=1}^{N} x(i))^2} \tag{10}$$

$$\frac{a}{c} = \frac{\sum_{i=1}^{N} x(i)^2 \sum_{i=1}^{N} b(i) - \sum_{i=1}^{N} x(i)b(i)\sum_{i=1}^{N} x(i)}{n\sum_{i=1}^{N} x(i)^2 - (\sum_{i=1}^{N} x(i))^2} \tag{11}$$

When two coefficients of mathematical model are obtained, the fitting curve is described as Fig.5.

Then the boundary of sea-sky region is decided by predefined belief values where smaller value decides the higher boundary of sea-sky area, and vice versa. Two probabilities are defined as P_{large} and P_{small} respectively. The relationship between belief values and the boundary of sea-sky region is shown as:

$$P_{large} = \frac{1}{1+e^{-(x_{low}-a)/c}} \tag{12}$$

$$P_{small} = \frac{1}{1+e^{-(x_{high}-a)/c}} \tag{13}$$

The upper boundary and lower boundary of sea-sky region are obtained:

$$x_{low} = a - c \times ln(\frac{1}{P_{large}} - 1) \tag{14}$$

$$x_{high} = a - c \times ln(\frac{1}{P_{small}} - 1) \tag{15}$$

Algorithm 1 Modifying method for eliminating outlier values

Input:
$Pro(i)$, $i = 1, 2, \ldots, N$, represents probability for being sea in each sub-region; N: the number of blocks.

Output:
$ModPro(i)$, $i = 1, 2, \ldots, N$, represents the verified probability.

```
while TRUE do
    flag = FALSE;
    for i = 1 to (N − 1) do
        if Pro(i) > Pro(i + 1) then
            Pro(i) = Pro(i + 1);
            flag = TRUE;
        end if
    end for
    if flag is equal to FALSE then
        break;
    end if
end while
```

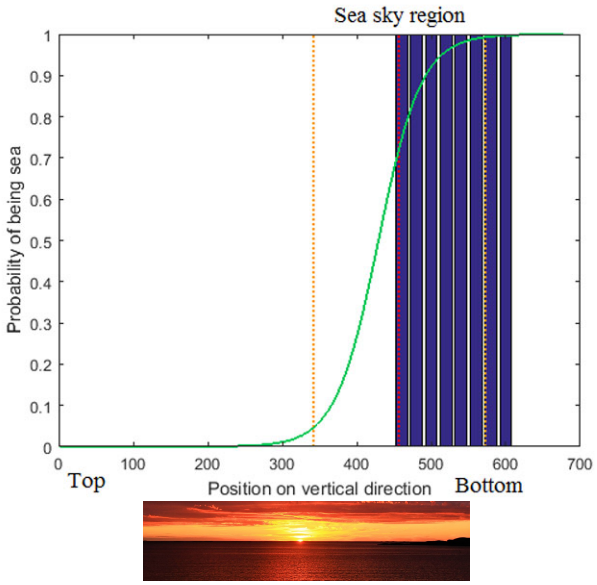

Fig. 5. Probability histogram and sea-sky region. X axis describes the position of each sub-region on vertical direction; Y axis is the probability of being sea (sea region has a larger probability); red line of dashes indicates the location of horizon line; sea-sky region is contained in yellow lines; green line is a curve fitted by positions of sub-regions with their corresponding probability; the image below is the final result of sea-sky region extraction.

The sea-sky region locates in interval $[x_{low}, x_{high}]$. In order to obtain enough area of sea and sky, this paper sets this paper sets $P_{large} = 0.99$, $P_{small} = 0.01$. Under this condition, sea-sky region is extracted as Fig. 5 shows. The model is constructed using least-squares method which eliminates outlier values and rectifies the probability distribution. Once the model is obtained, sub-regions with uncertain textural features are allocated the rectified probabilities by proposed model. Clouds on the sky or waves on the sea usually have stronger linear feature than the horizon. The irregular colour distribution disturbs the horizon detection. By sea-sky region extraction, the disturbance caused by waves and clouds will be reduced. Moreover, the horizon detection method is executed within a definite smaller area. It reduces the computational complexity and improves the processing rate of the horizon detection.

B. Horizon Estimation

For sea-sky region, Canny operator [26] is applied to extract edge information in sea-sky region which can reduce the computational complexity of Hough transform.

Hough transform can detect linear feature from a set of almost collinear figure points [25]. The algorithm is not prone to image noise and extracts aim precisely even if lines are discontinuous. The equation of a line is:

$$|\rho| = x\cos\beta + y\sin\beta \tag{16}$$

where $|\rho|$ is the distance of vertical line ρ from origin to fitted line; $\beta\epsilon[0,\pi)$ is the angle between x axis and ρ; (x,y) is a set points for linear fitting. For each (x_i, y_i) and its adjacent point, the parameters of line are obtained and the value of corresponding accumulator (ρ,β) increases by one. For every (ρ,β), larger value of accumulator represents a stronger linear feature, and vice versa. In [5], accumulator (ρ,β) with the largest value is supposed to be the parameter of real horizon. However it is hardly satisfactory to the most of situations where wave clutters often have stronger linear feature. Thus a set of lines corresponding the top M largest value of accumulator (ρ,β) are chosen as candidate horizons in Fig. 6. As the high clarity often comes with evident textural feature, the steep fitted curve in Fig. 5 indicates the clear image. Meanwhile the clear image of sea-sky region has a stronger linear feature for real. Under this circumstance, numeral value M is set to be smaller so as to reduce computational complexity. Inversely, in order to avoid the real horizon undetected, sea sky image with low clarity should choose more candidate horizons.

Fig. 6. Sea-sky region with M candidate horizons in green color.

Once these candidate horizon lines are acquired, a series of metrics are designed for determining the final real horizon. Different to the method MSCM [4], Hough transform in proposed method provides not only the linear feature, but also the locations of candidates on which the calculation of contextual physical characteristics is executed. At first, the linear feature of horizon is strong (may be not the strongest), which is described by accumulator of Hough transform. Therefore the value $Accu$ of accumulator is required as one of the metrics for horizon selection. Besides, the gray level of sky region and sea region are different and the sky region near the horizon has a lower weighted texture value than the sea region. The smoothness around candidate horizons can be evaluated by the standard deviation of gray level. The amount of variation or dispersion is smaller than it is in sea region. For every candidate horizon line, two 5×5 sliding windows are constructed above and blow the candidate horizon as Fig. 7 shows. The sliding window moves from leftmost to rightmost along the candidate horizon and the size of sliding step is set to 5. Within each sliding window, the following equations are computed.

$$gray_{5\times5} = \frac{1}{25}\sum_{i=1}^{5}\sum_{j=1}^{5} Win(i,j) \tag{17}$$

$$std_{5\times5} = \sqrt{\frac{1}{24}\sum_{i=1}^{5}\sum_{j=1}^{5}(Win(i,j) - gray_{5\times5})^2} \tag{18}$$

$$westd_{5\times5} = \frac{1}{gray_{5\times5}}\sqrt{\frac{1}{24}\sum_{i=1}^{5}\sum_{j=1}^{5}(Win(i,j) - gray_{5\times5})^2} \tag{19}$$

where $gray_{5\times5}$ is the average value of gray level; $Win(i,j)$ is gray level on the position of (i,j); $std_{5\times5}$ indicates standard deviation; $westd_{5\times5}$ represents weighted standard deviation. Vessels appearing on horizon will disturb the gray distribution and causes values in sky region larger. Hence only the minimum value on the sliding process is considered.

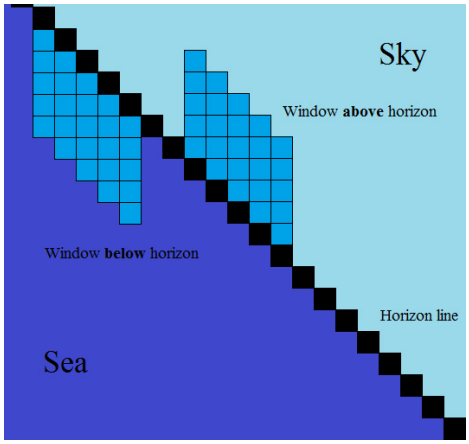

Fig. 7. Sliding windows above/below the horizon line.

According to these contextual features of horizon, a judgement combining with linear feature, average gray level as well as weighted standard deviation is devised as:

$$Eval = \frac{1}{(std_{up}+1)^{w_1}} \times Accu^{w_2} \times (westd_{down} - westd_{up})^{w_3} \tag{20}$$

where $Eval$ is the core of judgment for each candidate horizon; std_{up} is the smallest standard deviation within the window above candidate horizon, w_1 is the weighted value of std_{up}. $Accu$ indicates the accumulator value produced by Hough transform, w_2 is the corresponding weighted value. $westd_{down}$ is minimum weighted standard deviation created by windows above candidate horizon and $westd_{up}$ is the least weighted standard deviation produced by windows below candidate horizon whose weighted value is w_3. The candidate horizon line with the highest value of $Eval$ are considered as the real horizon. The result of horizon detection is shown as Fig. 8.

Fig. 8. The detecting result (white line) of horizon by proposed method.

III. Experimental Results

The performance of proposed horizon detection method is evaluated by comparison to other 5 state-of-art methods.The 5 methods are: the method using linear feature called H-HC [5]; the method based on discriminates and eigenvalues of covariance matrices in RGB space (H-DE) [16]; the method combining vectors and covariance matrices for color intensity (H-CI) [2]; the method adopting probability distribution functions of sea and sky region (H-PDF) [7] and the method by multi-scale cross modal linear feature (MSCM) [4].

TABLE I
Details of Datasets.

Dataset	Buoy [2]	Proposed	Singapore maritime [1]	
			Onboard	Onshore
No. of videos	10	10	10	35
No. of frames	996	1576	2915	16819
Min(Y-mean(Y))	-261.4424	-94.7219	-364.9797	-197.7587
Max(Y-mean(Y))	339.1325	223.6456	535.0281	395.6408
Standard deviation of Y	108.6655	55.8093	162.4086	103.7937
Min(θ-mean(θ))	-15.9123	-4.3847	-3.8498	-1.6998
Max(θ-mean(θ))	20.5301	3.0219	4.1307	3.969
Standard deviation of θ	4.4371	1.0318	1.8976	1.1653

The experiment is executed on three datasets: Singapore maritime dataset [1], Buoy dataset [2] and our proposed dataset including more than 20000 frames from electro-optical sensors under 65 different environments. The proposed dataset is created by Sony IMX179 with 6mm focal length. The sizes of frames vary from 720×365 to 1920×1080. According to the location of sensory, the test videos in datasets are divided in two categories: on shore and on board. For sensory on shore, the detected horizon is relatively stationary. But for the sensory mounted on board, the location of detected horizon changes along the vessel. Based on color distribution and textural feature, the frames of test videos are classified into blurred image and fine image. For fine image, there is an evident difference between the sky region and the sea region in color distribution. But for blurred image, the color distributions between two regions are similar. The blurred images are mainly caused by weather which often accompanies with thick clouds, sprays and splashed camera. Under this condition, the horizon detection would be influenced significantly. Besides, the occlusion caused by large vessels, vegetation and so on makes the horizon discontinued and the linear feature of the horizon become weak.

A. Evaluation criterion & Parameter setting

Several standards are proposed to describe the details of datasets and evaluate the performance of horizon detection method comparing to manual denoted results. At first, the angle θ between horizon and the horizontal edge of image, which indicates the inclination of horizon, is shown in Fig. 9. Y is the vertical distance from the center point of upper edge in the image to horizon and it is used to mark the location of horizon. The details of datasets are illustrated in Table I. The errors of angle θ and distance Y are produced by the subtraction of detected results and ground truth at every frame.

For i^{th} frame, the angle error θ_i^{error} and distance error Y_i^{error} is computed by:

$$\theta_i^{error} = \theta_i^{GT} - \theta_i \tag{21}$$

$$Y_i^{error} = Y_i^{GT} - Y_i \tag{22}$$

where θ_i^{GT} and Y_i^{GT} are the ground truth of horizon angle and location, respectively; θ_i and Y_i are detection results. Average errors are represented as:

$$\theta_{AE} = \frac{1}{Num} \sum_{i=1}^{Num} |\theta_i^{error}| \tag{23}$$

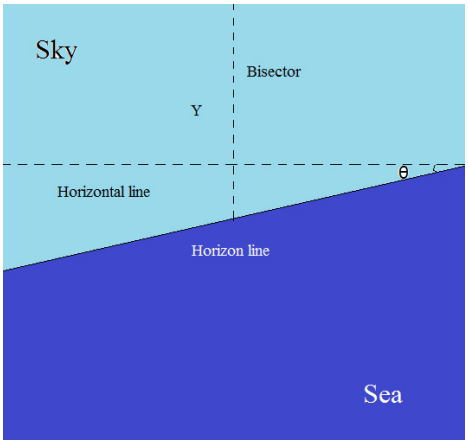

Fig. 9. The angle θ and distance Y in middle location of the horizon.

TABLE II
DETAILS OF PARAMETERS USED.

Number of sub-regions N=30
Probability interval [P_{small},P_{large}]=[0.01,0.99]
Size of sliding window: 5×5
If the extracted sea-sky region contains more than 5 sub-regions (include 5)
The number of candidates M=30, weighted values $w_1 = 1, w_2 = 2, w_3 = 1$;
else If the extracted sea-sky region contains less than 5 sub-regions
The number of candidates M=15, weighted values $w_1 = 3, w_2 = 5, w_3 = 1$.
Scale factors for Singapore maritime dataset [1] $Scale_{H-PDF} = 0.05, Scale_{H-DE} = 0.04, Scale_{H-CI} = 0.1$
Scale factors for Buoy dataset [2] and proposed dataset $Scale_{H-PDF} = 0.05, Scale_{H-DE} = 0.05, Scale_{H-CI} = 0.1$

$$Y_{AE} = \frac{1}{Num} \sum_{i=1}^{Num} |Y_i^{error}| \tag{24}$$

where Num is the total number of frames in test videos.

According to the physical characteristics under different environments, the parameters are set empirically by the number of sub-regions whose probability is between 0.01 and 0.99. To select values of w_1, w_2 and w_3, the image dataset containing nearly 200 different sceneries is constructed. The images are selected from dataset SMD [1], Buoy [2] and Internet. For fine image, the detection result is not sensitive to the change of weighted values. But for blurred image, both sea and sky have low textural complexity. Linear feature plays an important role in distinguishing sky from sea and corresponding weighted value w_2 should be increased. The selection of weighted values is based on experiment results. When the number of sub-regions in extracted sea-sky region is larger than 5, the amount of candidate horizon lines M=30, w_1=1, w_2=2, w_3=1; when the number is less than or equal to 5, the amount M=15, w_1=3, w_2=5, w_3=1. For method H-PDF, H-DE and H-CI with high computational complexity, the original frame should be set to be smaller. Because the size of frames in three datasets are different, corresponding scale factors are set so as to estimate the performances of methods under the approximate computational complexity. The details of parameters used on this experiment are demonstrated in Table II

TABLE III
ACCURACY RATE (%) OF SEA-SKY REGION EXTRACTION.

Dataset	Buoy [2]	Proposed	Singapore maritime [1]	
			Onboard	Onshore
Accuracy rate (%)	100	97.84	98.55	99.90

B. Results analysis

The proposed method could detect the horizon accurately only when the extracted sea-sky region contains the horizon. Occlusions appear near the horizon may have complex textural features. But the scattering effect weaken the influence caused by occlusions. As the extraction method is based on probabilities, the uncertainty brought by occlusions increases the size of extracted sea-sky region so as to include the horizon. To evaluate the effectiveness of sea-sky region extraction method, a strict standard is set that only the extracted sea-sky region containing the whole horizon is regarded as a correct extraction result. The accuracy rate of sea-sky region extraction by proposed method is shown in Table III. On some situations, even though the extracted sea-sky region contains a part of the horizon, the proposed method can detect the horizon accurately. In Fig. 10, the left image is the extracted sea-sky region while the right image is the result of horizon detection by proposed method.

Fig. 10. The extracted sea-sky region (left) and the result of horizon detection (right).

Based on 65 test maritime videos in Singapore maritime dataset [1], Buoy dataset [2] as well as proposed dataset, the performance of 6 methods are demonstrated from Table IV to Table VII. It can be concluded from Table IV and Table V that the proposed method has a better performance both in average center location error and in average angle error than other methods for all datasets. Although the average center location error produced by proposed method in dataset Onboard [1] is large, it is still tolerable comparing to the size of original video frame. But for other methods, they just satisfy some specific sceneries, e.g. method MSCM. It obtains a better detection result in Onshore dataset [1] however the detection results in centre location deviate far away from the ground truth in Onboard dataset [1].

In order to estimate the stability of horizon detection methods, the standard deviation on centre location error Y^{error} and angle error θ^{error} within each dataset are shown in Table VI and Table VII, respectively. As the detection error of proposed method is minimum, the amplitude of fluctuation around the ground truth is weaker than other methods. The

TABLE IV
AVERAGE CENTRA LOCATION ERROR Y_{AE} (IN PIXEL).

Methods	Dataset			
	Buoy [2]	Proposed	Singapore maritime [1]	
			Onboard	Onshore
MSCM [4]	4.2395	29.8490	218.2402	10.9713
H-CI [2]	139.2665	54.1815	50.9551	87.7430
H-HC [5]	6.1450	16.2821	132.7571	42.0757
H-PDF [7]	174.2168	100.5052	40.3386	43.3907
H-DE [16]	30.1506	130.6913	32.0536	40.2241
Proposed	**3.0944**	**4.8027**	**15.7981**	**7.0688**

TABLE V
AVERAGE ANGLE ERROR θ_{AE} (IN DEGREE).

Methods	Dataset			
	Buoy [2]	Proposed	Singapore maritime [1]	
			Onboard	Onshore
MSCM [4]	0.5627	0.8037	1.5096	0.3247
H-CI [2]	3.8630	3.3661	1.8975	1.8172
H-HC [5]	0.4079	0.4385	0.8753	0.3651
H-PDF [7]	6.7451	3.7588	2.4016	0.8765
H-DE [16]	3.4527	7.6170	3.8837	3.1037
Proposed	**0.3847**	**0.3338**	**0.4112**	**0.3124**

TABLE VI
STANDARD DEVIATION ON CENTRA LOCATION ERROR Y^{error}.

Methods	Dataset			
	Buoy [2]	Proposed	Singapore maritime [1]	
			Onboard	Onshore
MSCM [4]	**15.0124**	75.7566	214.6823	35.5998
H-CI [2]	116.2509	90.4617	85.3445	158.8357
H-HC [5]	33.2009	49.6421	209.1154	109.3672
H-PDF [7]	221.9335	117.0470	89.9382	126.1882
H-DE [16]	60.6384	119.0701	59.9874	55.4034
Proposed	17.6911	**14.6046**	**50.0784**	**13.4168**

TABLE VII
STANDARD DEVIATION ON ANGLE ERROR θ^{error}.

Methods	Dataset			
	Buoy [2]	Proposed	Singapore maritime [1]	
			Onboard	Onshore
MSCM [4]	0.7830	2.4718	2.2527	0.4380
H-CI [2]	5.1883	6.1459	2.8911	2.9519
H-HC [5]	**0.6015**	1.5125	1.5724	0.6409
H-PDF [7]	8.9383	5.2358	2.8667	1.5719
H-DE [16]	4.2080	10.3883	4.3988	4.0729
Proposed	0.6773	**0.9418**	**0.7229**	**0.4085**

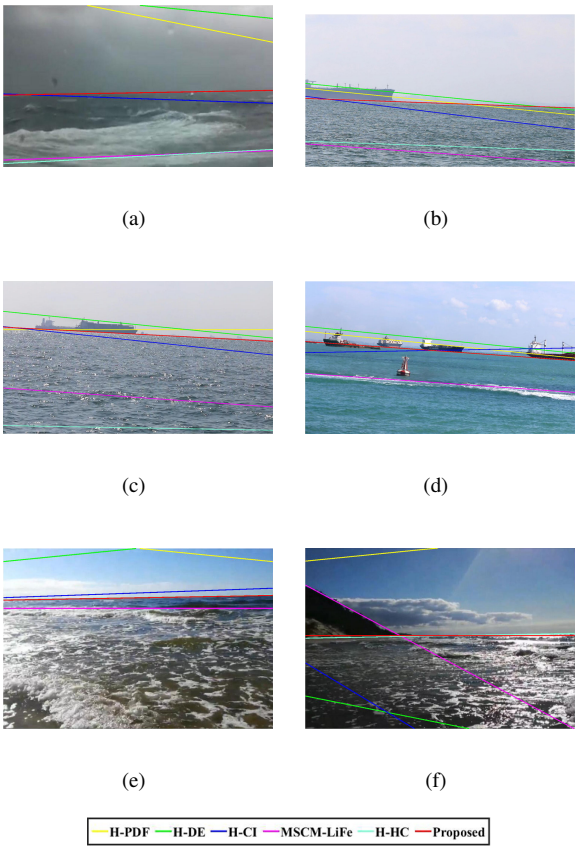

Fig. 11. The detection results by 6 methods.

Fig. 12. The example of false detection result by proposed method.

proposed method performs more stable and precise, whose margin of error is limited to a small range in center location and in angle. Both method H-HC [5] and method MSCM [4] have good performance in Buoy dataset [2]. But for other methods, no matter in center location or in angle, the detection results fluctuate more violently that heavily influences the practical application.

On Fig. 11 (a), the image is blurred whose gray distribution of sea and sky tends to be uniform. Thus, the methods based on RGB matrices (H-CI, H-PDF and H-DE) may not detect the horizon precisely. Besides, wave on the image has stronger linear features and lager intensity variation, which makes method MSCM ineffective. As for the in Fig. 11 (b) (c) (d) (f), the occlusion caused by vessels and mountains weakens linear feature of horizon. For Fig. 11 (e), light reflected from sea surface disturbs color distribution. With the help of physical characteristics around the horizon, the proposed method detects the horizon accurately.

But for image with large area of occlusion as Fig. 12 shown, the occlusion usually have strong linear feature. At the same time, the horizon is broken into several small parts with weak linear feature. Besides, the irregular structure and color distribution of occlusion could have similar physical characteristics to the horizon. As a result, the horizon is detected incorrectly in this kind of images.

IV. CONCLUSION

In this paper, a novel horizon detection method for maritime environment is proposed. The method is based on textural feature, linear feature, color as well as contextual information. It consists of sea-sky region extraction and horizon estimation, which have a superior performance even if the image is involved in complex factors (heavy wave, camera motion, occlusion, splashed camera, spray and thick clouds etc.). As the contributions of proposed method, new weighted textural metric and probabilistic interval-based model that

rectifies the outliers caused by occlusions, low-resolution etc. are used in sea-sky region extraction. Some physical characteristics around horizon are applied to select the final horizon.

As the vessels in long range always firstly appear near the horizon, sea-sky region is located with the help of the horizon for detecting vessels in maritime surveillance. However, it is not necessary to locate the horizon in proposed method. The first step of proposed method can directly extract the sea-sky region without extra computations. The experiments executed on a sequence of test videos demonstrate that the proposed horizon detection method has a higher accuracy and it is more robust as well as efficient than other existed methods. But for image with large area of occlusion on the horizon, all methods become ineffective. On the one hand, the occlusion with large area has strong linear feature and irregular color distribution. On the other hand, the linear feature of the horizon becomes weaker because of occlusion. Thus in future research, the combination of the semantic analysis with physical characteristics around the horizon will be interesting to detect the horizon from the complex background.

ACKNOWLEDGMENT

The authors would like to thank the support from China Scholarship Council (CSC).

REFERENCES

[1] D. K. Prasad, D. Rajan, L. Rachmawati, E. Rajabally, and C. Quek, "Video processing from electro-optical sensors for object detection and tracking in a maritime environment: a survey," *IEEE Trans. Intell. Transp. Syst.*, vol. 18, no. 8, pp. 1993-2016, Jan. 2017.

[2] S. Fefilatyev, D. Goldgof, M. Shreve, and C. Lembke, "Detection and tracking of ships in open sea with rapidly moving buoy-mounted camera system," *Ocean. Eng.*, vol. 54, pp. 1-12, Nov. 2012.

[3] X. Sun, Q, Xu, Y. Cai, M. Shi, and S. Li, "Sea sky line detection based on edge phase encoding in complicated background," *Acta. Opti. Sin.*, vol. 37, no. 11, pp. 1110002, Nov. 2017.

[4] D. K. Prasad, D. Rajan, C. K. Prasath, L. Rachmawati, E. Rajabally, and C. Quek, "MSCM-LiFe: Multi-scale cross modal linear feature for horizon detection in maritime images," in *Proc. Conf. IEEE Region 10 (TENCON)*, Nov. 2016, pp. 1366-1370.

[5] E. Gershikov, T. Libe, and S. Kosolapov, "Horizon line detection in marine images: which method to choose? ", *Int. J. Adv. Intell. Syst.*, vol. 6, no. 1 and 2, pp. 79-88, Jun. 2013.

[6] S. Fefilatyev, D. Goldgof, and C. Lembke, "Tracking ships from fast moving camera through image registration," in *Proc. 20th. Annu. Conf. ICPR*, Aug. 2010, pp. 3500-3503.

[7] I. Lipschutz, E. Gershikov and B. Milgrom, "New Methods for Horizon Line Detection in Infrared and Visible Sea Images", *Int. J. Comput. Eng. Res.*, vol. 3, no. 3, pp. 226-233, Mar. 2013.

[8] D. Liang, W. Zhang, Q. Huang, and F. Yang, "Robust sea-sky-line detection for complex sea background," in *Proc. PIC Conf.*, Dec. 2015, pp. 317-321.

[9] R. J. D. Moore, S. Thurrowgood, D. Bland, D. Soccol, and M. V. Srinivasan, "A fast and adaptive method for estimating UAV attitude from the visual horizon," in *Proc. IEEE Int. Conf. Intell. Robots. Syst.*, Sept. 2011, pp. 4935-4940.

[10] T. D. Cornall, G. K. Egan, and A. Price, "Aircraft attitude estimation from horizon video," *Electron. Lett.*, vol. 42, no. 13, pp. 744, Jul. 2006.

[11] S. J. Dumble, P. W. Gibbens, "Horizon Profile Detection for Attitude Determination," *J. Intell. Robot. Syst.*, vol. 68, no. 3-4, pp. 339-357, Jun. 2012.

[12] C. Liu, Y. Zhang, K. Tan, and H. Yang, "Sensor fusion method for horizon detection from an aircraft in low visibility conditions," *IEEE Trans. Instrum. Meas.*, vol. 63, no. 3, pp. 620-627, Mar. 2014.

[13] S. Thurrowgood, R. J. D. Moore, and D. Bland, "UAV attitude control using the visual horizon," in *Proc. Aust. Conf. Robotics. Autom.*, Dec. 2010.

[14] G.-Q. Bao, S.-S. Xiong, and Z.-Y. Zhou, "Vision-based horizon extraction for micro air vehicle flight control," *IEEE Trans. Instrum. Meas.*, vol. 54, no. 3, pp. 1067-1072, Jun. 2005.

[15] H. Zhang, P. Yin, X. Zhang, and X. Shen, "A robust adaptive horizon recognizing algorithm based on projection," *Trans. Inst. Meas. Control.*, vol. 33, no. 6, pp. 734-751, Feb. 2010.

[16] S. M. Ettinger, M. C. Nechyba, P. G. Ifju, and M. Waszak, "Vision-guided flight stability and control for micro air vehicles," in *Proc. IEEE Int. Conf. Intell. Robots. Syst.*, Oct. 2002, pp. 2134-2140.

[17] T. G. McGee, R. Sengupta, and K. Hedrick, "Obstacle detection for small autonomous aircraft using sky segmentation," in *Proc. Aust. Conf. Robotics. Autom.*, Apr. 2005, pp. 4679-4684.

[18] Y.-F. Shen, D. Krusienski, J. Li, and Z.-U. Rahman, "A Hierarchical Horizon Detection Algorithm," *IEEE Geosci. Remote. Sens. Lett.*, vol. 10, no. 1, pp. 111-114, Jan. 2013.

[19] J. Luo, S. Etz, "A physics-motivated approach to detecting sky in photographs," in *Proc. IEEE Int. Conf. Pattern. Recognit.*, Aug. 2002, pp. 155-158.

[20] A. Singhal, J. Luo, "Hybrid approach to classifying sky regions in natural images," in *Proc. Image. Video. Commun. Process.*, May. 2003, pp. 562-572.

[21] A. C. Gallagher, J. Luo, and W. Hao, "Improved blue sky detection using polynomial model fit," in *Proc. IEEE Int. Conf. Image. Process.*, Oct. 2004, pp. 2367-2370.

[22] J. Luo, S. P. Etz, "A physical model-based approach to detecting sky in photographic images," *IEEE Trans. Image. Process.*, vol. 11, no. 3, pp. 201-212, Mar. 2002.

[23] D. K. Lynch, W. Livingston, Color and Light in Nature. Cambridge, U.K.: Cambridge Univ. Press, 1995.

[24] D. Tang, G. Sun, D.-H. Wang, Z.-D. Niu, and Z.-P. Chen, "Research on infrared ship detection method in sea-sky background," *International Symposium on Photoelectronic Detection and Imaging: Infrared Imaging and Applications*, Sep. 2013.

[25] R. O. Duda, P. E. Hart, "Use of the Hough transformation to detect lines and curves in pictures," *Commun. ACM.*, vol. 15, no. 1, pp. 11-15, Jan. 1972.

[26] J. Canny, "A computational approach to edge detection," *IEEE Trans. Pattern. Anal. Mach. Intell.*, vol. PAMI-8, no. 6, pp. 679-698, Nov. 1986.

[27] A. Bhattacharrya, "On a measure of divergence between two multinomial population," *Sankhya. A.*, vol. 7, no. 4, pp. 401-406, Jul. 1946.

[28] Y. Xu, J. Wen, L. Fei and Z. Zhang, "Review of video and image defogging algorithms and related studies on image restoration and enhancement," *IEEE Access.*, vol. 4, pp. 165-188, Dec. 2015.

[29] C. F. Bohren, D. R. Huffman, Absorption and Scattering of Light by Small Particles New York: Wiley, 1983.

[30] C. Y. Jeong, H. S. Yang and K. D. Moon, "Fast horiozn detection in maritime images using region-of-interests," *Int. J. Distrib. Sens. N.*, vol. 14, no. 7, pp. 1-11, Jul. 2018.

[31] C. Y. Jeong, H. S. Yang and K. D. Moon, "Horizon detection in maritime images using scene parsing network," *Electron. Lett.*, vol. 54, no. 12, pp. 760-762, Jun. 2018.

[32] D. K. Prasad, D. Rajan, L. Rachmawati, E. Rajabally and C. Quek, "MuSCoWERT: multi-scale consistence of weighted edge Radon transform for horizon detection in maritime images," *J. Opt. Soc. Am. A. Opt. Image. Sci. Vis.*, vol. 33, no. 12, pp. 2491-2500, Dec. 2016.

[33] Y. Sun, L. Fu, "Coarse-fine-stitched: a robust maritime horizon line detection method for unmanned surface vehicle applications", *Sensors*, vol. 18, no. 9, pp. 1-18, Aug. 2018.

Dong Liang received the B.E. degree from the Harbin Institute of Technology, Weihai, China, in 2016, and the M.S. degree in computer science from the National Technical University, Kharkiv, Ukraine, in 2018. His current research interests include image processing, computer vision, machine learning and knowledge graph.

Ya Liang received the B.E. degree from Guangxi Universtity, Nanning, China, in 2011, and the M.S. degree from Shandong University, Jinan, China, in 2014. Since then, she has been a lecturer at Weihai Ocean Vocational College. Her research interests include biomedical instrumentation and applications and ocean science.